19th International Conference on the Computation of Electromagnetic Fields

Technical Program

Compumag 2013

30 June–4 July 2013, Budapest, Hungary

	PC2-20 **Evaluation of Singular Integral Equation in MoM Analysis of Arbitrary Wire Structures** Maicon Vaz Moreira, Ursula do Carmo Resende, Marcio Matias Afonso Federal Center for Technological Education of Minas Gerais, Brazil **PC2-21** **A Novel Approach to Deal with Rotationally Symmetrical Conditions for 3D Eddy Current Field Problems** S. L. Ho[1], Shiyou Yang[2] [1]The Hong Kong Polytechnic University, Hong Kong; [2]Zhejiang University, People's Republic of China **PC2-22** **Domain Decomposition Method used in Reducing Error near Boundaries Based on Combined RBF Collocation** Yang Zou[1], K. R. Shao[1], Xiaoming Chen[1], Gang Lei[2], Youguang Guo[2], Jianguo Zhu[2] [1]College of Electrical and Electronic Engineering, Huazhong University of Science and Technology, China; [2]Faculty of Engineering and information technology, University of Technology, Australia
10:35am - 12:15pm **Corvina**	**PC3: Electrical Machines & Drives 3** **Session Chairs:** Karl Hollaus, Stanislaw Gratkowski
	PC3-1 **Design of Saliency-based Sensorless Controlled IPMSM with Concentrated Winding for EV Traction** Myung Seop Lim[1], Seung Hee Chai[1], Byeong Hwa Lee[1], Jung Pyo Hong[1], Jung Ik Ha[2] [1]Hanyang university, Republic of Korea (South Korea); [2]Seoul National univeristy, Republic of Korea (South Korea) **PC3-2** **A Novel Calculation Method on the Current Information of Vector Inverter for Interior Permanent Magnet Synchronous Motor for Electric Vehicle** Ki-Chan Kim Hanbat National University, Republic of Korea (South Korea) **PC3-3** **Improvement of Convergence Behavior for Steady-State Analysis of Permanent Magnet Synchronous Motor** Hirokatsu Katagiri, Yoshihiro Kawase, Tadashi Yamaguchi Gifu University, Japan **PC3-4** **Airgap Reluctance Identification for the Magnetic Equivalent Circuit Modelling of Induction Machines** Johan Gyselinck[1], Ruth V. Sabariego[2] [1]Université Libre de Bruxelles (ULB), Belgium; [2]Université de Liège (ULg), Belgium **PC3-5** **Pole-Changing of DC-Excited Dual-Memory Machines** Fuhua Li, K.T. Chau, Chunhua Liu, Christopher H.T. Lee, Mu Chen The University of Hong Kong, Hong Kong S.A.R. (China)

Design of Saliency-Based Sensorless Controlled IPMSM with Concentrated Winding for EV Traction

Myung-Seop Lim[1], Seung-Hee Chai[1], Jung-Pyo Hong[1], *Senior Member, IEEE* and Jung-Ik Ha[2]

[1]Department of Automotive Engineering, Hanyang University, Seoul 133-791, Korea
[2]School of Electrical and Computer Engineering, Seoul National University, Seoul 151-742, Korea

This paper presents the design process of a sensorless-oriented interior permanent magnet synchronous motor (IPMSM) with concentrated winding, based on spatial saliency for traction in electric vehicles. The purpose of the design method is to ultimately achieve both stable rotor position detection and acceptable mechanical performances, under the maximum load conditions. After describing the evaluating procedure of sensorless control viability, the geometry design parameters are analyzed to figure out which ones have a positive effect on sensorless drive. Focusing on the parameter analysis, a prototype and improved model are proposed. Optimization is conducted, using response surface methodology (RSM) with the factors selected by design of experiment (DOE). Finally, the validity of the design results is verified by comparison with the simulations and the tests. It is founded that the accuracy of the rotor position estimation and mechanical characteristics can be improved simultaneously by means of the proper geometry design.

***Index Terms*—Cogging torque, cross-coupling effect, high frequency injection, sensorless control, spatial saliency, torque ripple.**

I. Introduction

TODAY, an interior permanent magnet synchronous motor (IPMSM) is usually employed as electric vehicle (EV) traction because of its high torque density. To achieve the best performance of the machine, a position sensor is essential for vector control. However, this addition increases the system cost, volume and complexity, and decreases reliability of the machine. In addition, using the position sensor could be a latent critical defect of an IPMSM, especially, for a traction application. This is because if the sensor is in default, the driver cannot control the vehicle resulting in danger. For these reasons, design method of an IPMSM for sensorless drive is critical.

In an IPMSM, permanent magnets (PM) have an effect on not only induced back EMF, but spatial saliency distribution. Non-uniformly positioned PM in the rotor causes a discrepancy between the *d* and *q*-axis impedance. This is because the *d*-axis flux path is saturated easily by the magnetic flux and the high *d*-axis reluctance due to the low permeability of the PM. This result brings about the spatial saliency. Therefore, with a high-frequency signal injection method, the position of the rotor can be estimated based on the saliency [1]. As shown in Fig. 1, if the voltage injection angle is 0 degree when the voltage is injected on the *d*-axis, the *d*-axis self-inductance has a minimum value and the *dq*-axis mutual-inductance must be zero because of the impedance. However, it is not easy to estimate the rotor position under load conditions, since the inductance is distorted by input current or cross-coupling effect [2]-[5]. Thus, sensorless drive feasibility is predicted by evaluating the shifting of zero-crossing point of the *dq*-axis inductances with a rotor position [4].

In this paper, some design factors (notch, chamfer, eccentricity and pole angle) are analyzed with design of experiment (DOE). Through the design optimization of the parameters, an improved model is proposed, fulfilling sensorless drive viability and low cogging torque/torque ripple. Lastly, the validity of the simulation results is verified by comparison with the experimental results of the prototype.

Manuscript received January 1, 2013. Corresponding author: Jung-Pyo Hong (e-mail: hongjp@hanyang.ac.kr).
Digital Object Identifier inserted by IEEE

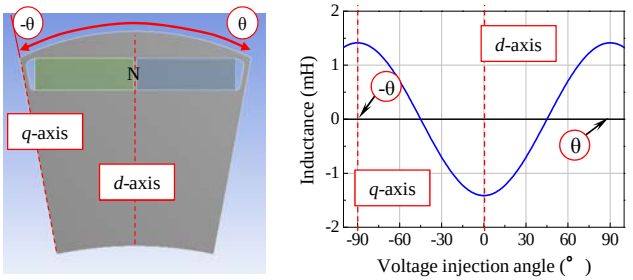

Fig. 1. *d*-axis inductance waveform under no-load condition

II. Computing of the Inductances for Evaluating Saliency-Based Sensorless Drive Feasibility

A. Fixed Permeability Method

The fixed permeability method is used for calculating the inductances mentioned above. Fig. 2 shows the process of this method to find a phase inductance. The first step is finite element analysis (FEA) including permanent magnets. At this time, nonlinear FEA has to be done, considering the saturation of the core. The next step is fixing the permeability of each element. After this, linear FEA is conducted with eliminating the PM. At this point, by injecting the 1-phase coil with the unit current, the self and mutual inductance can be obtained. This process should be iterated by rotating the rotor, because the waveform (or zero-crossing point) of the *dq*-axis inductance is varied with the rotor position.

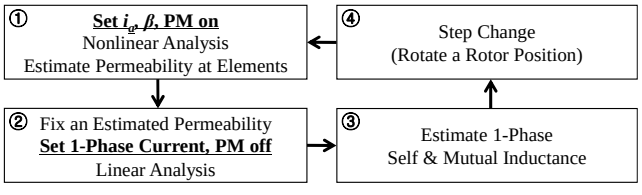

Fig. 2. Flow chart of the fixed permeability method

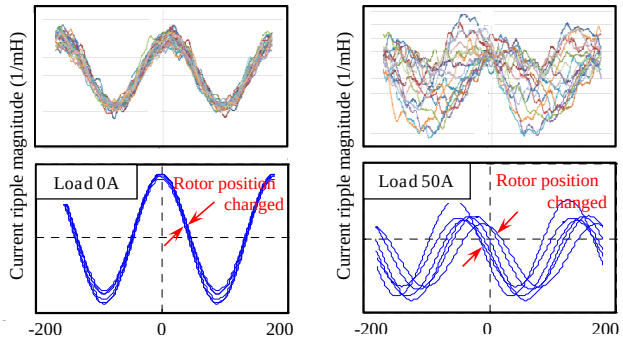

(a) No-load condition (b) 50A load condition

Fig. 3. Estimated current ripple (lower) and experimental result (upper)

B. *Matrix Transformation of the Inductances*

With (1), a 3-phase inductance matrix determined by the fixed permeability method can be transformed to *d*, *q*-axis inductances depending on voltage injection angle.

$$L_{dq}^{r} = \frac{3}{2} T_{\theta_r} T_{dq} L_{AB} \left(T_{\theta_r} T_{dq} \right)^{T} = \begin{bmatrix} L_d & L_{dq} \\ L_{qd} & L_q \end{bmatrix} \quad (1)$$

where L_{AB} is the 3-phase inductances including space harmonics. T_{dq} and $T_{\theta r}$ are the *d*, *q* axis transform and the rotational transform coefficient. L_d, L_q, L_{dq} and L_{qd} are the *d*- and *q*-axis self- and mutual-inductances. Fig. 3 illustrates the variation of the *d*-axis current ripple (inverse values of L_d) with the rotor position under no-load and load conditions.

III. Analysis of the Design Parameters for a Sensorless-Oriented IPMSM

A. *Magnetic Load and Electric Load*

If possible, sensorless-oriented motors should have the same *d*, *q*-axis inductance waveforms as the rotor position under load conditions. Thus, it requires sinusoidal flux distribution and minimum flux distortion by armature reaction at the air gap. This means that a machine has to be designed to have a higher magnetic load than electric load as much as possible for in order to take advantage of sensorless drive. In (2) and (3), the magnitude of magnetic load and electric load are described. *B*, L_{stk}, N_{ph} and D_r are the flux density, stack length, number of turn phase and rotor diameter respectively. The pole-pair number and the number of phase are *p* and *m*.

$$\phi = B \times \frac{\pi D_r L_{stk}}{2p} \quad (Wb) \quad (2)$$

$$A = \frac{2mN_{ph}I}{\pi D_r} \quad (A/m) \quad (3)$$

B. *Design Parameters in the Rotor and Stator*

In this paper, some design parameters are analyzed to find out their effects on a sensorless-oriented machine. For quantification of sensorless control feasibility, phase

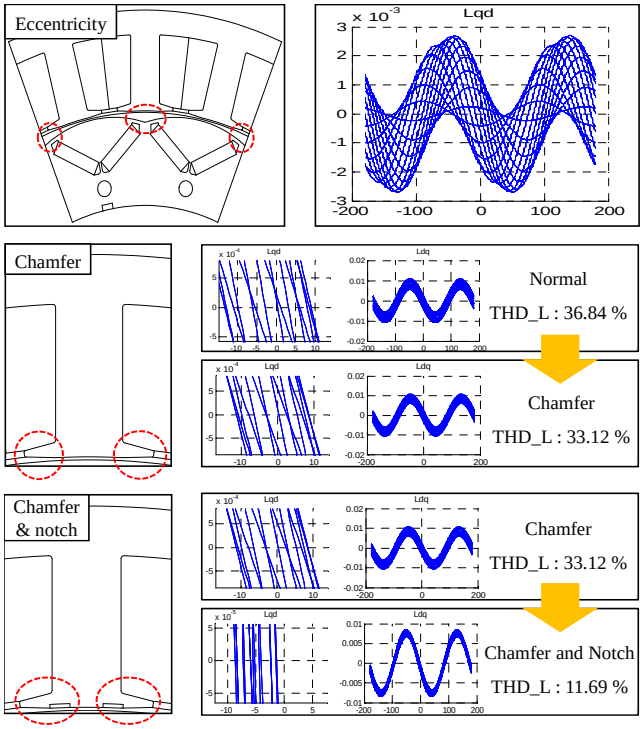

Fig. 4. Design factors and the *dq*-axis inductances (THD_L: phase inductance THD)

inductance total harmonic distortion (THD) is used. This is because phase inductance space harmonics cause variation of the L_d, L_q, L_{dq} and L_{qd} waveforms with the rotor position. The results of FEA under the maximum load conditions are described in Fig. 4. Eccentricity has a negative effect on the sensorless drive. Pole angle is not considerably related to it. The point is that chamfer and notch have a positive effect on the sensorless control. Given this analysis, it can be inferred that the shape of the tooth-tip in the stator is closely related to the performance of the saliency-based sensorless drive. Furthermore, it shows that saturating the tooth-tip is one of the key factors for concentrated winding sensorless drive machine.

C. *Prototype (16pole-24slot, 115Nm-14kW)*

A prototype, motor with chamfer only, is shown in Fig. 5(a). Fig. 5(b) illustrates variation of L_{dq} waveform with the rotor position under the maximum load conditions. It is expected that the sensorless control for the prototype is viable since the variation level of L_{dq} is not high. However, saturation of the tooth-tip causes its high cogging torque and torque ripple (cogging torque; peak to peak: 14.96Nm, torque ripple: 12.92%). Therefore, an additional design process is required.

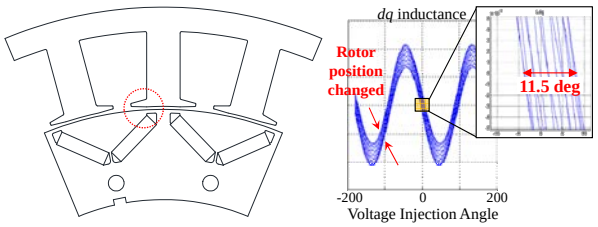

Fig. 5. Sensorless-oriented prototype (left), and the variation L_{dq} waveforms with the rotor position (electrical angle: 0~180 degree) (right)

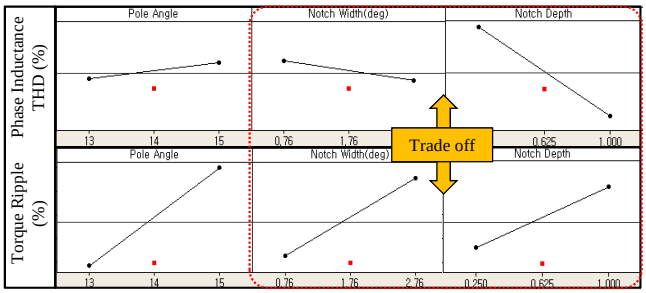

Fig. 6. Main effect of each parameter (left: pole angle, mid: notch width, right: notch depth)

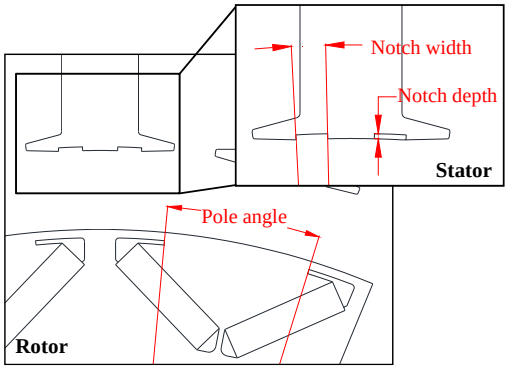

Fig. 7. Design parameters for DOE

IV. Design of the Improved Model

A. Response Surface Methodology

Statistical experimental methods such as design of experiment (DOE) and response surface methodology (RSM) were applied to optimize the media. RSM is a collection of statistical techniques for designing experiments, building models, evaluating the effects of various parameters and searching for the optimum condition [6], [7]. A quadratic approximation function of the models is commonly used to constrict the fitted response surface. In general, the response model can be written as follows [8].

$$Y = \beta_0 + \sum_{i=1}^{k} \beta_i x_i + \sum_{i=1}^{k} \beta_{ii} x_i^2 + \sum_{i \neq j}^{k} \beta_{ij} x_i x_j + \varepsilon \qquad (4)$$

where β are the regression coefficients for the design variables, and ε is the random error treated statistical error.

The fitted coefficients and the fitted response model by using the least square method which is used to estimate unknown coefficients can be written as

$$\hat{\beta} = (X'Y)^{-1} X'Y \qquad (5)$$

$$\hat{Y} = X\hat{\beta} \qquad (6)$$

where X is the matrix notation of the levels of the independent variables, X' is the transpose of the matrix X, $\hat{\beta}$ is the matrix of the fitted coefficient, and $\hat{Y}$ is the vector of the observations.

There are many experimental designs for the creation of the response surfaces. Design of experiment for fitting the second-order response surface must involve at least three levels of each variable. Therefore, to build the second-order fitted model, the central composite design (CCD) is used. CCD is frequently used for fitting a second-order response model [6].

Before conducting RSM, the full factorial design (FFD) has to be done [8]. Given the result in Fig. 6, notch size causes a trade-off relation between phase inductance THD and torque ripple. However, pole angle is not considerably related to sensorless control, but significantly affects cogging torque and torque ripple [9]. Thus, the optimized combination of notch width and depth, and pole angle is essentially required for achieving both the least error of the rotor position estimation and low cogging torque/torque ripple. These are the reasons that notch width and depth, and pole angle were selected as optimal design parameters for RSM as shown in Fig. 7. In addition, the objective functions are back electromotive force (BEMF), phase inductance THD, cogging torque and torque ripple. Fig. 8 describes the results of RSM. The white area in the figure is the optimal design region. The values of the parameters meet the requirements (optimal design point) that should be decided in that area.

B. Improved Model (16pole-24slot, 115Nm-14kW)

The improved model and the *dq*-axis inductances under the maximum load conditions are shown in Fig. 9. The values of the optimal parameters are as follows. Pole angle: 12degree, Notch width: 1.90degree, Notch depth: 0.56mm. The rotor position could be estimated more precisely than the prototype thanks to hardly shifting zero-crossing points of L_{dq}. Furthermore, the improved model has much lower cogging torque and torque ripple (cogging torque; peak to peak: 5.85Nm, torque ripple: 5.78%).

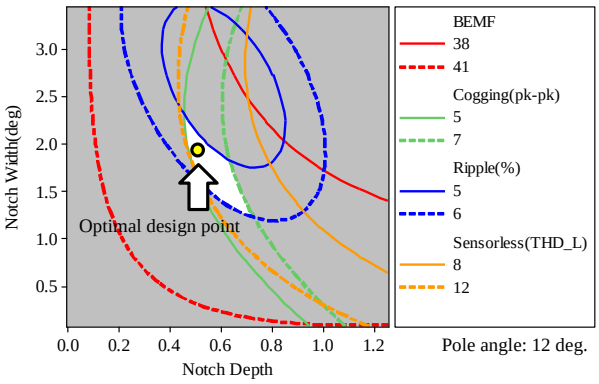

Fig. 8. Result of the response surface methodology and the target region of the design parameters

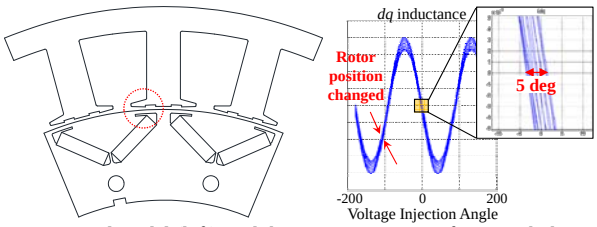

Fig. 9. Improved model (left), and the variation L_{dq} waveforms with the rotor position (electrical angle: 0~180 degree) (right)

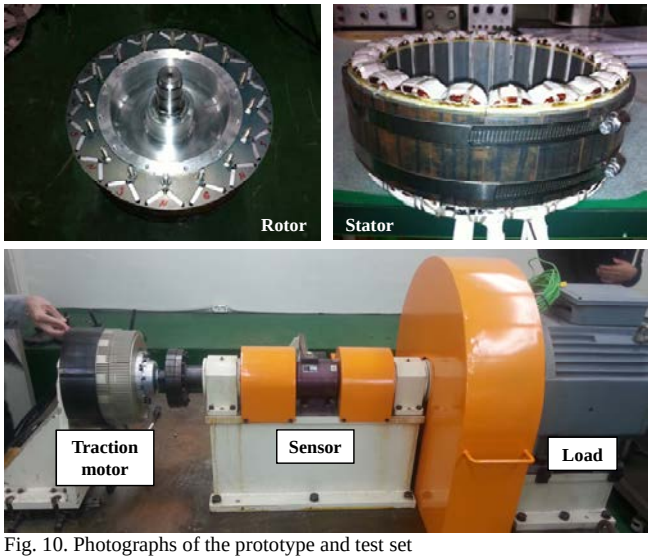

Fig. 10. Photographs of the prototype and test set

V. Experimental Verifications and Design Results

The prototype is fabricated as shown in Fig. 10. It was tested to verify the validity of the result acquired by FEA and the proposed design method in this paper. Table I demonstrates the reliability of the FEA results. In addition, the errors between the estimated and actual rotor position are quite small as shown in Table II. Given the torque test result in Fig. 11, thanks to the small position errors, the torques are only slightly different when the machine is operated with a sensor and sensorless drive. Finally, characteristics of the improved model and the prototype are compared in Fig. 12.

VI. Conclusion

In this paper, design parameters were examined to clarify the design procedure of sensorless drive concentrated winding IPMSM. As a result, saturating the tooth-tip is one of the key factors for designing a sensorless-oriented motor. However, the saturation of the tooth-tip gives rise to high cogging torque and torque ripple. Hence, with the parameters selected by FFD such as notch size and pole angle, RSM is conducted. Consequently, not only are cogging torque and torque ripple decreased about 61% and 55%, but the shifting of the *dq*-axis inductances' zero-crossing or phase inductance THD, representing sensorless drive feasibility, is reduced by 56%.

TABLE I

FEA and Experimental Results of the Prototype (25℃)

	BEMF [V]	Cogging torque [Nm]
FEA	44.60	21.38
Experiment	45.33	20~22

TABLE II

Position Error at the Steady State of the Prototype

Speed [rpm]	*q*-axis current				
	140A	98A	0A	-98A	-140A
0	-1.3deg.	1.3deg.	0.9deg.	0.7deg.	0.9deg.
200	-1.3deg.	0.4deg.	1.9deg.	1.0deg.	-1.1deg.

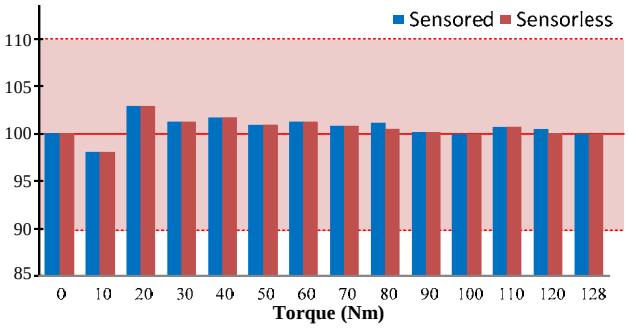

Fig. 11. Torque accuracy test at 200rpm of the prototype (*y*-axis: torque accuracy (%))

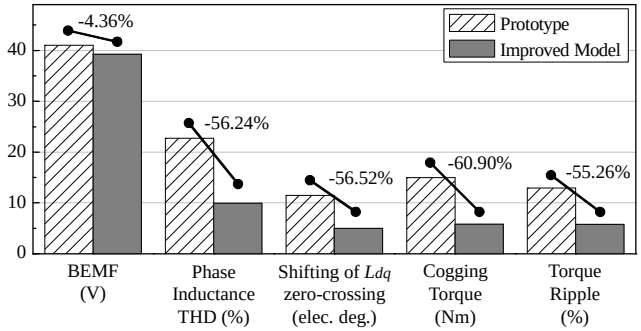

Fig. 12. Comparison of FEA between two models as design results (100°C)

Acknowledgment

This research was supported by the MKE (The Ministry of Knowledge Economy), Korea, under the CITRC (Convergence Information Technology Research Center) support program (NIPA-2013-H0401-13-1008) supervised by the NIPA (National IT Industry Promotion Agency).

References

[1] S. M. Kim, J. I. Ha and S. K. Sul, "PWM switching frequency signal injection sensorless method in IPMSM," *IEEE Trans. on Ind. Appl.*, vol. 48, No. 5, pp. 1576-1587, 2012.

[2] Y. Kano, T. Kosaka, N. Matsui and M. Fujitsuna, "Sensorless-oriented design of concentrated winding IPM motors for HEV drive application," *in conf. Rec. IEEE ICEM*, pp. 2709-2715, 2012.

[3] Y. Li, Z. Q. Zhu, D. Howe and C. M. Bingham, "Modeling of cross-coupling magnetic saturation in signal-injection-based sensorless control of permanent-magnet brushless AC motors," *IEEE Trans. Magn.*, vol. 43, No. 6, pp. 2552-2554, June, 2007.

[4] Z. Q. Zhu, Y. Li, D. Howe and C. M. Bingham, "Compensation for rotor position estimation error due to cross-coupling magnetic saturation in signal injection based sensorless control of PM brushless AC motor," *in conf. Rec. IEEE IEMDC*, pp. 208-213, 2007.

[5] N. Bianchi and S. Bolognani, "Influence of rotor geometry of an IPM motor on sensorless control feasibility," *IEEE Trans. on Ind. Appl.*, vol. 43, No. 1, pp. 87-96, Jan.-Fab., 2007.

[6] B. H. Lee, J. P. Hong, J. H. Lee and S. M. Jang, "Optimum design criteria for maximum torque and efficiency of a line-start permanent-magnet using response surface methodology and finite element method," *IEEE Trans. Magn.*, vol. 48, No. 2, pp. 863-866, Feb. 2012.

[7] J.T. Li, Z.J. Liu, M.A. Jabbar and X.K. Gao, "Design optimization for cogging torque minimization using response surface methodology," *IEEE Trans. Magn.*, vol. 40, No. 2, pp. 1176-1179, 2004.

[8] Sung-Il Kim, Jung-Pyo Hong, Young-Kyoun Kim, Hyuk Nam and Han-Ik Cho, "Optimal design of slotless-type PMLSM considering multiple responses by response surface methodology," *IEEE Trans. Magn.*, vol. 42, No. 4, pp. 1219-1222, April 2006.

[9] Y. Kano, T. Kosaka, N. Matsui and T. Nakanishi, "Design and experimental verification of a sensorless-oriented concentrated-winding IPMSM," *in conf. Rec. IEEE ICEM*, pp. 1-6, Sept., 2010.